

Coplanar Waveguide Passive Components on Ceramic AlN Substrates for Application in Hybrid Integrated X-band GaN-based High-Power Amplifiers

Mark Krämer, Roger Hoskens, Bart Jacobs, Erwin Suijker¹, Peter de Hek¹, Thieu Kwaspen, Fouad Karouta and Leon Kaufmann

Technische Universiteit Eindhoven, Department of Electrical Engineering,
Inter-University Research Institute COBRA, Opto-Electronic Devices Group
EH 8.16, P.O. Box 513, 5600 MB Eindhoven, The Netherlands
Phone: +31 (0)40 247 5116, Fax: +31 (0)40 244 8375

E-mail: m.c.j.c.m.kramer@tue.nl

¹TNO Physics and Electronics Laboratory, The Hague, The Netherlands

Abstract— We have investigated coplanar waveguide (CPW) passive components on ceramic AlN substrates for application in hybrid integrated X-band GaN-based high-power amplifiers. CPW technology becomes crucial if a via-hole technology is not available. A set of processed transmission lines (TLs), discontinuities, metal-insulator-metal (MIM) capacitors and resistors has been used for the extraction of scalable models. These elements are embedded between two adaptors for RF probing. We have developed a technique to de-embed the adaptors from the overall measurement in order to correctly determine the properties of the element itself. Measurements on elements containing multiple ports with right angles can best be carried out using standard calibration techniques followed by carefully re-orienting the probes. It is shown that for accurate design of matching networks operating at 10 GHz each element has to be carefully modeled. An inaccuracy of less than 5% between measured and modeled S-parameters at X-band for a fabricated CPW demonstrator circuit proves the validity of the scalable models for CPW passive circuit design in this frequency band.

Keywords— AlN; Amplifiers; CPW; Hybrid integration; Passive components

I. INTRODUCTION

We are working towards hybrid integrated X-band (8 – 12.4 GHz) GaN-based high-power amplifiers. Using this integration scheme the active devices, AlGaIn/GaN high electron mobility transistors (HEMTs) grown on sapphire or SiC substrates, will be connected by flip-

chip technology to the coplanar waveguide (CPW) passive circuits on ceramic AlN substrates that provide the matching and biasing of the HEMTs. The passive circuits consist of transmission lines (TLs), discontinuities (90° bends, crosses, T-junctions), metal-insulator-metal (MIM) capacitors and thin film Nickel-Chromium (NiCr) resistors. Ceramic AlN is a very good candidate to serve as substrate material for our application because of its excellent thermal and electrical properties besides the fact that it is very cheap. These substrates however eliminate the possibility of using microstrip technology because this technology requires via holes. Therefore, we have used CPW technology in which both the signal line and ground planes are located on top of the substrate. The fact that via holes are not needed simplifies fabrication. In addition, the elimination of the parasitic source inductance associated with via holes enables gain enhancement for CPW amplifiers circuits. A drawback of CPW technology is that it is less well implemented in commercial design software than microstrip. Besides the process technology needed for the fabrication of CPW circuits we have developed a de-embedding technique to determine the properties of the individual passive components in order to develop scalable models.

II. PROCESS TECHNOLOGY

All passive components have been processed on ceramic AlN substrates. The sample area and thickness

are $15 \times 15 \text{ mm}^2$ and $508 \text{ }\mu\text{m}$ respectively. The maximum surface finish of the polished substrates is 25 nm . The processing starts with the deposition of 50 nm Silicon Nitride (SiN_x) to promote the adhesion of the photoresist. Standard lift-off lithography and e-beam metal evaporation are used to define TLs, bottom and top plates of the MIM capacitors. The dielectric in the MIM capacitors is formed by 200 nm PECVD SiN_x . The thickness of the evaporated TLs is $2 \text{ }\mu\text{m}$ which is enough to reduce losses and provide sufficient current carrying capability. Two-step lithography and e-beam evaporation are used to fabricate airbridges. Thin film resistors are fabricated using a 125 nm sputtered Nickel-Chromium (NiCr) layer. These resistors are aged and passivated in order to stabilize their resistance value.

III. DE-EMBEDDING CPW LINES

The general layout of a typical CPW TL test structure is illustrated in Figure 1. The structure consists of a TL connected to an adaptor on either side. This adaptor is necessary because not every line is suitable for probing. Also, because the elements are on a different substrate than the calibration substrate and the metal geometry around the probe is different, one cannot assume a perfect RF connection between probe and line. The adaptor accounts for all the effects mentioned above.

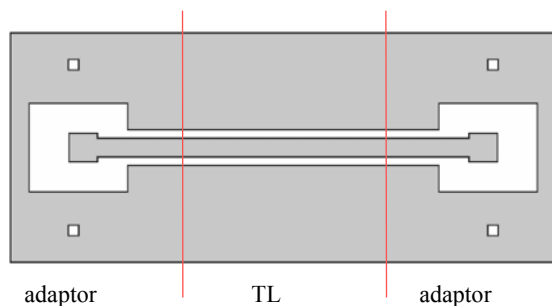


Figure 1 Schematic layout of a CPW TL test structure.

The addition of the two adaptors makes it impossible to determine the characteristics of the intrinsic line element from an arbitrary number of measurements of structures like the one illustrated in Figure 1. To fully characterize the TL one needs additional measurements. These measurements can be in the form of connecting a short or an open instead of one of the two adaptors. The problem with this approach is the difficulty of realizing a perfect open or short at high frequencies ($>10 \text{ GHz}$). To bypass these problems we have chosen to follow the approach published by Pantoja [1] and Marks [2]. We model the adaptor by a pi-equivalent circuit as shown in

Figure 2. This approach is valid for passive reciprocal two-ports.

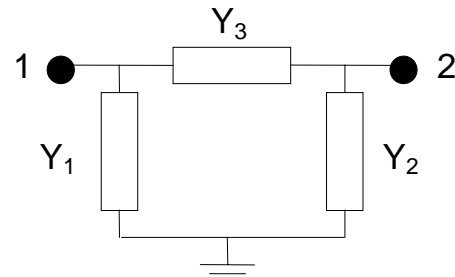


Figure 2 Equivalent circuit of an adaptor.

We start off by measuring two TLs. The first line consists of two adaptors in series. We shall denote the measured ABCD parameters of this line by T . A second measurement of a line with a length l_{delay} of for instance $1000 \text{ }\mu\text{m}$ is measured. The ABCD parameters of this line are multiplied by T^{-1} to give the matrix D . Using these line measurements and notations, one can express the line characteristics, meaning the characteristic impedance Z_0 and the propagation constant γ , as a function of the Y_3 parameter of the adaptor:

$$Z_0^{-1} = Y_3^2 (\frac{1}{2} T_1 D_{11} + \frac{1}{2} (T_0 - 1) D_{12} - \frac{1}{2} T_1 G_0) / (G_0^2 - 1)^2 \quad (1)$$

$$\gamma = \text{acosh}(G_0) / l_{\text{delay}} \quad (2)$$

In which G_0 is obtained from:

$$G_0 = \frac{1}{2} (T_0 + 1) D_{11} - \frac{1}{2} (T_0 - 1) D_{22} + \frac{1}{2} D_{12} T_2 - \frac{1}{2} D_{21} T_1 \quad (3)$$

This indicates that an additional measurement is needed to solve for Y_3 . The propagation constant however can be determined from these two measurements alone. According to classical waveguide theory [3], we can express Z_0 as a function of the line inductance L [H/m], capacitance C [F/m], conductance G [S/m] and resistance R [Ω /m] according to:

$$Z_0 = ((R + j\omega L) / (G + j\omega C))^{0.5} \quad (4)$$

Similarly the propagation constant can be written as:

$$\gamma = ((R + j\omega L)(G + j\omega C))^{0.5} \quad (5)$$

Assuming that the dielectric losses (G) can be neglected compared to the line capacitance, we can combine these relations to give:

$$Z_0 = \gamma / j\omega C \quad (6)$$

Measuring the difference in capacitance of the two TLs at relatively low frequencies (< 1 GHz) and dividing this by l_{delay} gives the line capacitance. Using the equations for Z_0 one can determine the properties of both the TL and the adaptor.

Figure 3 shows an example of the characteristic impedance as a function of frequency for a CPW TL with a signal line width of $45 \mu\text{m}$ and a signal to ground spacing of $75 \mu\text{m}$. Assuming that the propagating mode in the CPW line is a true quasi-TEM mode, analytical solutions for the line properties can be found [4].

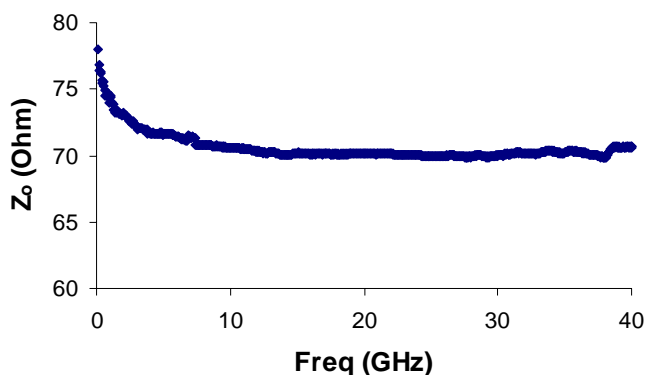


Figure 3 Typical result for the characteristic impedance of a CPW TL.

Table 1 shows a comparison between the analytical formulas and the measured values. A very good agreement is obtained proving the validity of our approach. Other CPW elements will also have adaptors connected to either side. Once the properties of the adaptors have been determined we can de-embed them from every subsequent element.

Table 1: Comparison between measured values for the line-capacitance (C_{exp}) and values based on the quasi-TEM approach (C_{qtem}) for different signal line widths (w) and signal to ground spacings (s).

w [μm]	s [μm]	C_{exp} [pF/m]	C_{qtem} [pF/m]
45	75	99	97.4
20	100	71	73.3
100	20	183	179.6
35	20	138	134.8
70	75	110	110.1
50	45	118	116.4
75	45	132	130.7
85	100	105	107.3

IV. ORTHOGONAL STRUCTURES

Other CPW elements like Tee's and crosses present another difficulty. These elements contain right angle bends that require a right angle calibration. Figure 4 shows an example of right angle bends in the case of a processed CPW Tee. Most calibration substrates contain right angle line elements but mostly these structures cannot be used for accurate calibration. To illustrate this point we have conducted two measurements of a CPW bend. One measurement was carried out using a right angle SOLT (short-open-line-through) calibration, for the other measurement we performed a 'normal' LRM (line-reflect-match) calibration followed by carefully reorienting the probes to perform the right angle measurement.

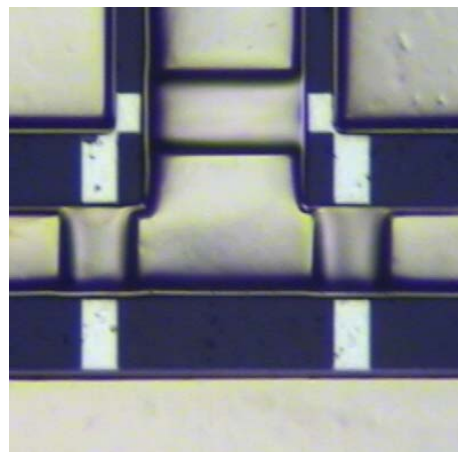


Figure 4 Example of a CPW Tee showing the right angles in the device.

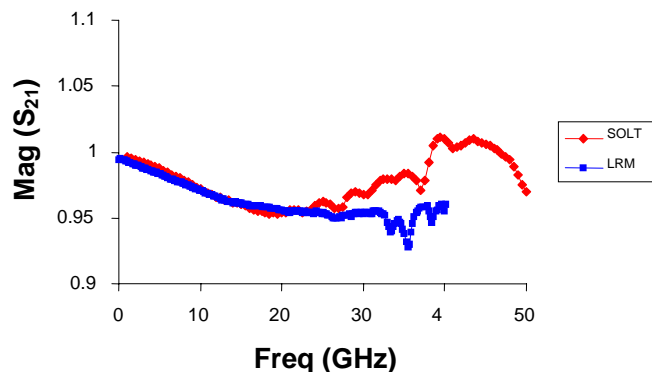


Figure 5 Comparison of the S_{21} parameter of a right angle bend using a right-angle SOLT calibration and a 'normal' LRM calibration.

Figure 5 shows the measured S_{21} parameter of the bend. In the case of the right-angle calibration S_{21} becomes larger than 1, which of course is not valid for a passive structure. Carefully re-orienting the probes with the cables seems to be the best option for measuring right-angled structures.

V. CAPACITORS AND RESISTORS

To complete the set of CPW passive components we processed NiCr thin film resistors and MIM capacitors. The layouts for these elements, together with a schematic cross-section, are shown in Figures 6 and 7, respectively.

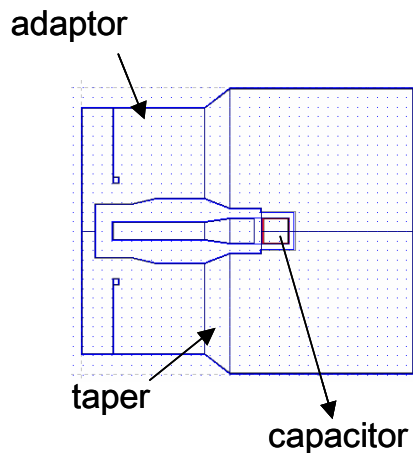


Figure 6 Layout for a capacitor to ground. Note the taper between the adaptor and the actual capacitor.

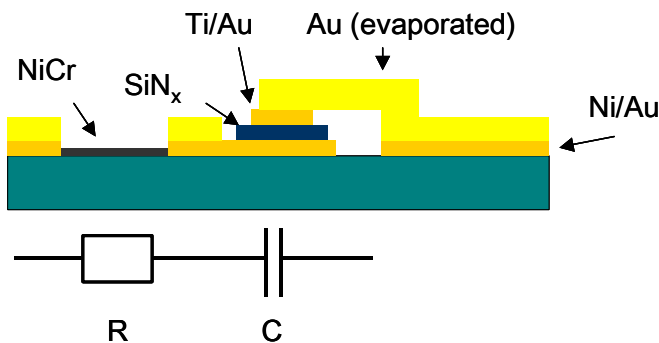


Figure 7 Schematic cross-sectional view of a NiCr thin film resistor and MIM capacitor in series.

Using a NiCr layer thickness of 125nm we obtained a sheet resistance of $8 \Omega/\text{sq}$. after aging and passivation. The MIM capacitance scales with the surface of the top plate giving a capacitance density of $0.2\text{nF}/\text{mm}^2$. Both the resistor and capacitor contain two tapers that

transform the connecting line geometry in the geometry of the NiCr line or the bottom plate of the capacitor. These tapers, which have a length of $100 \mu\text{m}$, result in an extra inductance in series with the resistor/capacitor. The equivalent circuit shown in Figure 8 can model both the resistor and capacitor. The first three elements on either side model the tapers, although C_3 and C_4 contain the input capacitance of the resistor/capacitor part as well.

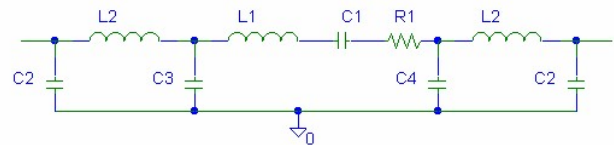


Figure 8 Equivalent circuit for capacitor/resistor.

The tapers in series with the capacitor constitute a series resonance circuit. The effective capacitance can be approximated by:

$$C_{\text{eff}} = C_0 / (1 - (\omega/\omega_r)^2) \quad (7)$$

Where C_0 is the low-frequency capacitance and $\omega_r = 1/(LC_0)^{0.5}$ the resonance frequency of the circuit in which L models the inductance of the tapers.

This resonance behavior can clearly be seen in the measurements. Figure 9 shows $-Y_{12}/j\omega (=C_{\text{eff}})$ for a series capacitor after the adaptors were de-embedded. For capacitors above 0.3 pF , C_{eff} significantly differs from C_0 . This shows that designing a matching network with these elements requires accurate models for both the tapers and the actual capacitor/resistor.

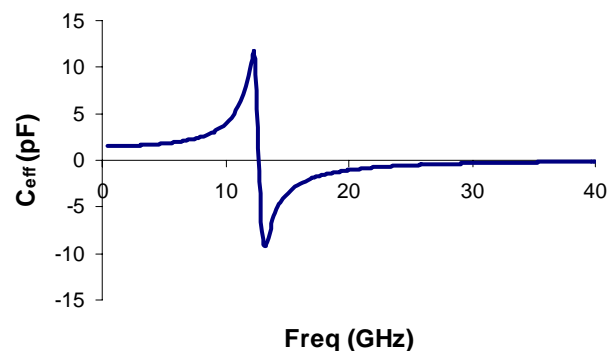


Figure 9 MIM capacitor with a top plate of $75 \times 75 \mu\text{m}^2$ (1.5 pF). The resonance occurs in the X-band.

VI. DEMONSTRATOR CIRCUIT

For all CPW components we have developed scalable models [5]. These models have been extracted from a set of fabricated elements with different geometries and by using the previously described de-embedding technique and the conformal mapping results as obtained by Heinrich. To verify these models we have fabricated several demonstrator circuits at X-band, e.g. a 2-to-1 combiner. Figure 10 shows its schematic layout.

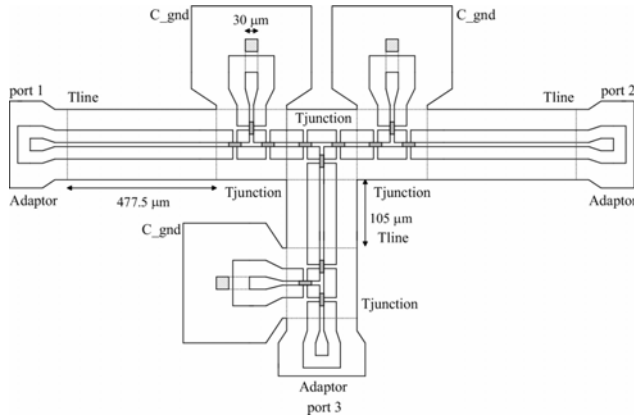


Figure 10 Schematic layout of the 2-to-1 combiner circuit.

This circuit provides the matching of 25Ω at ports 1 and 2 to 50Ω at port 3. A comparison between measurements and simulations based on our scalable models is shown in Figures 11 and 12. Figure 11 shows that the difference between measured and modeled transmission data is only 0.5 dB at X-band. Moreover, the exact frequencies of the resonance peaks around 34 GHz differ only 2 % as can be seen in Figure 12.

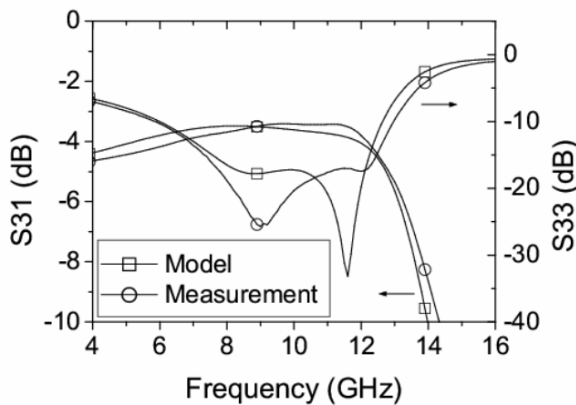


Figure 11 Magnitude of S_{31} and S_{33} at X-band.

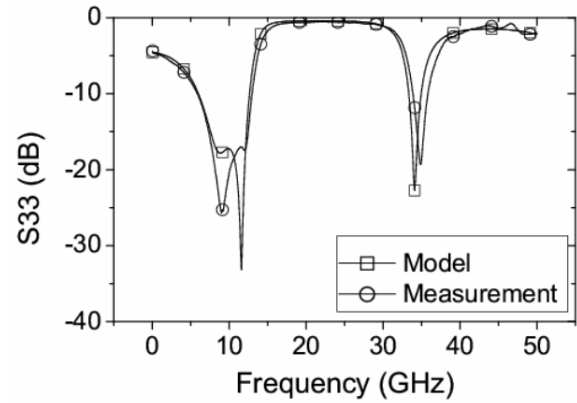


Figure 12 Measured and modeled values for the magnitude of S_{33} up to 50 GHz.

Figures 11 and 12 show that the inaccuracy between measured and modeled data is less than 5% for the relevant S-parameters at X-band which demonstrates the validity of the scalable models.

VII. CONCLUSIONS

In this paper we have discussed our CPW process technology on ceramic AlN substrates. Furthermore, we have presented a method to correctly determine the properties of CPW elements needed in matching networks for X-band AlGaIn/GaN high-power amplifiers. To remove the influence of the adaptors needed for probing a de-embedding technique has been developed. Using this method we are able to determine the CPW TL properties that show excellent agreement with analytical formulas based on quasi-TEM solutions. Elements containing right angles like a bend or a cross need to be calibrated using standard through calibrations followed by carefully re-orienting the probes. It has been shown that using right-angled calibration structures gives erroneous results. Comparison of measured and modeled transmission and reflection data for the 2-to-1 combiner demonstrator circuit indicates the validity of the scalable component models and their applicability for CPW passive circuit design at X-band.

VIII. ACKNOWLEDGMENT

The authors would like to thank the Dutch Technology Foundation STW for their financial support of this research under project NAF 5040. Furthermore, they would like to thank TNO Physics and Electronics Laboratory for both their technical and financial support.

REFERENCES

- [1] R.R. Pantoja, "Improved Calibration and Measurement of the S-parameters of Microwave ICs", *IEEE Microwave Theory and Techniques*, Vol. 37, pp. 1675-1680, 1989.
- [2] R.B. Marks and D.F. Williams, "Characteristic impedance determination using propagation constant measurement", *IEEE Microwave Guided Wave Letters*, Vol. 1, pp. 141-143, 1991.
- [3] D.M. Pozar, "Microwave Engineering", Wiley, New York, 1999
- [4] W. Heinrich, "Quasi-TEM description of MMIC coplanar lines including conductor-loss effects", *IEEE transactions on microwave theory and techniques*, Vol. 41, no. 1, pp. 45-52, 1993.
- [5] B. Jacobs, "Towards Integrated AlGaIn/GaN Based X-Band High-Power Amplifiers", *PhD thesis*, Eindhoven University of Technology, 2004.